Understanding the impact of standardized SAE waveform parameter variation on artificial lightning plasma, specimen loading and composite material damage

Understanding the impact of standardized SAE waveform parameter variation on artificial lightning plasma, specimen loading and composite material damage

Abstract

Previous works have established strategies to model artificial test lightning plasma with specific waveform parameters and use the predicted plasma behavior to estimate test specimen damage. To date no computational works have quantified the influence of varying the waveform parameters on the predicted plasma behavior and resulting specimen damage. Herein test standard Waveform B has been modelled and the waveform parameters of 'waveform peak', 'rise time' and 'time to reach the post-peak value' have been varied. The plasma and specimen behaviors have been modelled using the Finite Element (FE) method (a Magnetohydrodynamic FE multiphysics model for the plasma, a FE thermal-electric model for the specimen). For the test arrangements modelled herein it has been found that 'peak current' is the key parameter influencing plasma properties and specimen damage. A 10% increase in peak current magnitude (and resulting 21% increase in action integral) results in a 12% increase in plasma peak pressure, a 5% increase in specimen surface current density, and subsequently a 8.7% increase in thermal damage volume and a 15.2% increase in thermal damage depth. Overall action integral has the strongest correlation with four of the five considered damage measures. Peak current has the strongest correlation with the other damage measure.

Keywords

Lightning Strike; Magnetohydrodynamics; Aerospace Materials; Thermal Plasma; Finite Element Modelling; Composite Damage; Correlation Factors.

1.0 Introduction

On average lightning strikes interact with an aircraft once per year, approximately every 3,000 hours, during their operating period [1]. A lightning strike is a complex, naturally occurring phenomenon that involves the interaction of many physics, including fluid, electrical and thermal behavior. During a lightning strike a plasma is generated due to rapid ionization of the air and an arc channel at temperatures upwards of 10,000^{o}C is formed [2]. Lightning strikes have been characterized into four test Waveforms (A, B, C and D) for use in experimental and simulation research, proposed in SAE-ARP5412B [3]. Each of these waveforms can last between micro to milliseconds and have varying peak currents.

A limited number of published experimental works exist for test lightning strikes due to the cost and specialist test infrastructure involved [1], [4]–[17]. FE and CFD simulations have been developed to model the plasma and damage produced during a typical test lightning strike [8], [17]–[26]. Plasma simulations using FE or more recently CFD and based on Magnetohydrodynamics (MHD) can be traced back to gas tungsten arc (GTA) welding processes or general free burning arcs [27]–[34]. MHD combines three distinct sets of partial differential equations; Maxwell's equations of electromagnetism, Navier-Stokes equations of fluid motion, and thermal conduction equations for heat transfer to model the mutual interaction between fluid flow and magnetic fields.

Authors have also used FE modelling to predict the likely damaged composite specimen due to incident current, temperature or pressure loading [17], [18], [20], [22], [23], [25], [35]–[37]. However, recently measures have been taken to combine plasma modelling and specimen material damage predictions [21], [24], [35], due to the complexity and computational burden of the required models. Thus limited understanding exists on the influence of plasma modelling on the prediction of specimen damage, and vice versa. This paper aims to understand the impact of the key Waveform parameters ('waveform peak', 'rise time' and 'time to reach the post-peak value') on the formation of artificial test lightning plasma; to relate this to specimen loading and subsequent specimen material damage; and to do this using established modelling approaches and a structured study technique.

2.0 Background

2.1 Lightning strike experimental research

Lightning strike experimental research is based on the standardized waveforms noted in the introduction. Waveform A is characterized as the first return stroke; Waveform B is the intermediate current; Waveform C is the long continuing current; and Waveform D is a subsequent stroke [3], where each waveform is defined using six parameters. These are peak current, I_{peak} (kA), the rise time from 10% to 90% of the maximum current, T1 (ms), the time to reach the post-peak value of 50% of the maximum current, T2 (ms), the peak rate-of-rise (kA/ms), the charge transfer (C) and its action integral (A^2s). The greatest volume of works have conducted experiments on composite specimens with a waveform parameter scaled from Waveform A [1], [4], [6], [14], [16], [17], with only a very few works conducting experiments considering multiple or sequential strikes with different waveforms [5], [15]. Some other works have focused on strikes on aluminum panels [10]–[12].

A small number of authors have sought to correlate specimen damage with waveform parameters through experimental investigation [1], [6], [11], [13]. However, given the cost and challenges associated with experimental work and the large number of interrelated parameters and variables, the development of experimental correlations has been somewhat restricted.

Hirano et al. [1] incorporated eight test conditions, modifying waveform time period, peak current, action integral and specimen stacking sequence. Hirano et al. [1] found, for the selected experimental arrangement and test specimen design, that peak current had the greatest influence over fiber damage area and thickness while charge and action integral governed the area of delamination and resin deterioration respectively. Kawakami [6], with a similar waveform but different specimen materials, found that action integral and peak current were the greatest contributors to damage depth but the relationships were non-linear. Kostogorova-Beller [11] [12] also studied the influence of specimen thickness but in this case used aluminum specimens, Waveform C, and correlated charge and current amplitude with damage area. Hirano et al. [1] used a least square error regression method to determine the largest R^2 for each waveform parameter/damage measure pair. Kawakami [6] and Kostogorova-Beller [12] plotted the data

and used a best fit line to determine if the relationship between pairs of parameters was linear or exponential, while Hosokawa et al. [13] simply plotted the data points.

No experimental studies have been able to relate the variation of waveform parameters to the plasma properties or specimen loading, attempting only to link waveform parameters directly to damage measures. It would be possible, with significant data, to systematically calculate correlation coefficients to quantify the relationships between waveform parameters and damage measures [38], [39]. However, such an approach is absent from the experimental literature and significantly would not include the plasma parameters.

Considering plasma behavior, very limited experimental work is available on the influence of waveform parameters on the lightning plasma properties. Sonehara et al. [40] attempted to visually observe the behavior occurring between the discharge probe and the specimen using high-speed video cameras and Schlieren photography. In this work, two electrodes were compared with both CFRP and Aluminum specimens under five test conditions. An increase in applied peak current was shown to increase the temperature and velocity of the plasma produced. Interestingly, this behavior has never been computationally replicated as an aid to verify the capability of plasma simulations.

2.2 Lightning arc plasma modelling

Plasma simulations considering lightning strikes have been designed to replicate the experimental works discussed previously, with many works modelling the setup of reference [1]. In these simulations a conical electrode was modelled along with the test specimen allowing specimen loading conditions to be calculated and not assumed. As noted in the introduction, MHD is primarily used to represent the plasma behavior and welding process simulations, e.g. [34], and were initially adapted to represent the artificial lightning test conditions used to create the strike plasma.

Plasma models have been developed for artificial test lightning waveforms A, B and C [19], [24], [26] enabling the calculation of the conditions on the top surface of the test specimen under action of the applied Waveform current. Wang et al. [19] generated a 3D lightning plasma CFD model for Waveform

C. In this model a copper specimen was used. Chen et al. [24], also using CFD, generated a model for Waveform A with a CFRP specimen. However, both of these models used an imposed temperature boundary condition of 3500 K to incorporate a formed plasma channel and an assumed initial electrical conductivity.

Abdelal and Murphy [26] used an FE based modelling approach to simulate Waveform B with a copper conical electrode and copper specimen. Similitude theory was used to employ scaling and therefore reduce the run time of the simulation. Of particular note in this work was the use of a 1D electron transport model to predict air electric conductivity removing the need for an initial temperature boundary condition assumption. This enabled the prediction of initial plasma channel attachment to the specimen surface starting from room temperature conditions.

Millen et al. [21], using Abdelal and Murphy's [26] model, varied specimen properties and examined the influence on the predicted plasma. However, in this work the waveform was held constant as a standard Waveform B profile. Millen et al. and Chen et al. are the only authors to couple their plasma model with a specimen damage model, however, both authors modelled a single, fixed waveform [24], [35].

In summary, a benefit of modelling the lightning plasma is the potential to capture the impact of changing waveform parameters on the formation of the lightning plasma and the loading conditions on the specimen. While variation in specimen properties has been studied through simulation, there has been no consideration of variation in waveform properties. Such study has been limited to experimental works with no capture of plasma properties. No studies, experimental or simulation based, have captured the influence of the waveform parameters on both the plasma and specimen damage in a quantifiable manner. The use of simulation to generate data sets for the calculation of correlation coefficients is a viable approach to understand the complicated interacting physics between the lightning waveform parameters and the resulting lightning plasma. Such models would also enable the calculation of loading conditions on the specimen surface for the examination of specimen damage.

2.3 Specimen thermal-electric modelling

Lightning strike thermal damage simulations have been developed with varying meshes and loading methods used within these simulations [17], [20], [22], [24], [25], [35], [41]. Ogasawara et al. [20] were the first authors to present a clear thermal-electric simulation for Waveform A, replicating the experimental work of Hirano et al. [1]. Abdelal and Murphy [25] improved this method with the addition of temperature dependent material properties. Foster et al. [22] added arc expansion and movement to better represent behavior observed in experiments, again representing the experimental work of Hirano et al. [1].

Chen et al. [24] and Millen et al. [35] sequentially coupled their previously discussed plasma simulations to thermal damage models. Chen et al. [24] coupled the simulations using a volume spline function, Millen et al. [35] coupled the simulations using a python scripting method. Both authors were able to predict damage area and depth by using temperature boundaries corresponding to CFRP decomposition and ablation temperature limits, similar to previous work [22]. Millen et al. [21] in a further study presented damage models with different material structures, unprotected, epoxy protected and copper protected. Most of these authors have used the same material data sets and model boundary conditions.

Two authors have done simulations to correlate waveform properties with damage within the thermal-electric simulation domain. Dong et al. [42] developed a coupled thermal-electric-pyrolytic model to analyze lightning waveform properties and their effect on composite laminates. Yin et al. [43] modelled the interaction of lightning Waveform D parameters with the extent of ablation damage. Like other authors in the field, damage area, damage depth and volume were all presented. Both groups of authors found that action integral increased the damage area and depth. However, both sets of authors used assumed specimen surface loading conditions equal to the Waveform profile under investigation, rather than the specimen surface loading resulting from the lightning plasma.

This work will attempt, for the first time, to establish the influence of percentage variations in waveform parameters (specifically time periods and peak current magnitudes), on the percentage

variation in plasma properties (peak pressures, velocities, temperatures, currents), and link these to percentage variations in the specimen damage (depths, areas, volumes). This will be done for a simulated Waveform B event. Appropriate data sets will be generated to calculate correlation coefficients to quantify the complicated interacting physics between the lightning waveform parameters, the generated lightning plasma and the ultimate specimen damage mechanics.

3.0 Methodology

3.1 Waveform Test Cases and Plasma Simulation

The key waveform properties which were varied were the time periods T1/T2 and the peak current. In this system, waveform properties were increased by 10% or maintained at the baseline levels. 10% variation was chosen to be sufficiently large to produce different profiles but not large enough to change the test waveform character or encroach on the other waveforms. A 2^2 level analysis was used and generated four test cases as shown in

Table 1. While a three level analysis would have allowed for the determination of quadratic relationships between the factors and results this would have been computationally prohibitive as each plasma simulation lasted for approximately ten days and would have required an additional five simulation runs. The potential presence of curvature in the relationships will be determined with a simple analysis of the R^2 values.

A naming convention was generated to allow convenient determination of waveform properties through this manuscript without repeated reference to the relevant figures. The convention is as follows; $PC^mT^mA^n$, where *PC* represents peak current, *T* is the time periods T1/T2, *A* is the action integral with a value *n* (*n* x 10^4 (A^2s)) and *m* is either = or + where = represents no change and + represents +10% change in the relevant property.

The first and reference plasma model ($PC^=T^=A^{2.85}$) represents the standard Waveform B parameters. The loading of the model was governed by the base waveform equation (Equation 1):

$$I(t) = I_0\left(e^{-\alpha t} - e^{-\beta t}\right)(1 - e^{-\gamma t})^2 \qquad (1)$$

where I_0 is 11,300 A, α is 700s^{-1}, β is 2000s^{-1}, γ is 22,000s^{-1} and *t* is time (s). For the subsequent models the time periods were adjusted in this equation by modifying the exponential factors and the peak current magnitude was increased by scaling the entire waveform by 10%.

This simulation incorporated MHD, Navier-Stokes equations, Maxwell equations, thermal conduction equations, the Newton–Raphson method and boundary conditions which replicated the previous works which developed and verified the modelling approach [26], [35] and replicated the modelling approach to study its sensitivity [21]. All simulations employed similitude theory to minimize the computational cost and each simulation featured an unprotected specimen and conical tip electrode (Fig. 1) which replicated the experimental arrangement of Hirano et al. [1]. The mesh used in these plasma simulations is shown in Fig. 2.

Results from the plasma model were then passed to the thermal-electric simulations. The four modelled input waveforms for the plasma simulations can be seen graphically in Fig. 3 and the relevant waveform properties for each of the four test waveforms is presented in

Table 1. It should be noted that all waveforms had a fixed total duration of 5ms and thus all had differing total energy inputs. This is in line with the preceding experimental works which varied the time periods and peak currents and permitted the total waveform energy to vary (i.e. magnitudes of charge transfer and action integral) [1].

3.2 Thermal-electric damage modelling

The thermal-electric simulations modelled the experimental specimen of Hirano et al. [1] with IM600/133 composite material, with a layup of $[45/0/-45/90]_{4s}$ and measured 150 × 100 × 4.704 mm. In all analyses a transient, fully coupled, thermal-electric step using the Newton–Raphson method was used with DC3D8E elements [44]. In this step electrical loading was applied and resistive heating occurred within the specimen. Temperature dependent material properties were used in each analysis, and are presented in Table 2. The same zero electrical potential boundary conditions were applied to the side and bottom surfaces of the specimen to replicate experimental conditions where the composite specimen was set on a copper plate [1]. The simulation mesh was generated and converged in accordance with the temperature boundary methods used in previous publications of this type [22], [35]. Details of the mesh convergence procedure can be found in reference [35] and the final mesh is presented in Fig. 4. The electrical loading was applied, using a python scripting method, to the center of the specimen, using multiple surface current loads. Again for brevity the details of the simulation coupling method are not repeated herein but can be found in [35].

4.0 Results

First the four case study results will be presented examining plasma behavior before considering the specimen temperature contours and the resultant specimen damage (focusing on the damage surface area, volume and depth). The results will be compared in a pairwise fashion to enable understanding of how waveform peak magnitude and waveform rise and fall (T1/T2) influence individual plasma and surface properties. It should also be noted that the applied action integral and charge transfer were changing in each case (

Table 1) and very careful analysis is required between the cases. The comparisons will necessarily consider differences between peak magnitudes (independent of time) and also at single fixed times, for example at T1.

In order to better understand the relationships between the input waveform parameters, plasma peak properties and the surface peak properties correlation coefficients [38], [39] between the individual pairs of variables will be presented. The calculation of correlation coefficients assumes a linear relationship between the studied variable pairs and will be discussed further once the results have been presented. Correlation coefficients are divided into ranges signifying different levels of linearity within the data; 0 indicates no linear relationship, +1 indicates a perfect positive linear relationship, -1 indicates a perfect negative linear relationship, 0 to 0.3 (0 to -0.3) indicates a weak positive (negative) linear relationship, 0.3 to 0.7 (0.3 to -0.7) indicates a moderate positive (negative) linear relationship and values between 0.7 and 1.0 (-0.7 and -1.0) indicate a strong positive (negative) linear relationship [39].

4.1 Comparison of waveform properties and predicted plasma

1. Comparison of peak current

Comparing Cases $PC^{=}T^{=}A^{2.85}$ and $PC^{+}T^{=}A^{3.44}$, Table 3, it can be seen that an increase in the peak current of the incident waveform produced an increase in the plasma peak fluid properties. The plasma peaks in temperature and pressure occurred 0.01ms earlier with the increase in peak current. At the same time point (*time=1ms*) the plasma temperature, pressure and velocity were greater for case $PC^{+}T^{=}A^{3.44}$ by 1.02%, 7.25% and 5.29% respectively. This behavior was also observed at the specimen surface, Table 4, with all surface peak loads increasing with the increase in peak current. Generally with the greater peak current load ($PC^{+}T^{=}A^{3.44}$), the surface load peaks occurred further from the arc center, due to the increase in the plasma surface velocity with the exception of peak surface temperature which always occurred at the arc center for all cases.

Comparing Cases $PC^{=}T^{+}A^{3.15}$ and $PC^{+}T^{+}A^{3.82}$, Table 3, peak plasma properties all increased with the peak plasma pressure occurring later and peak plasma temperature and velocity occurring earlier. The

surface loads also increased, as before, with the peak surface pressure, current density and velocity all occurring further from the arc center.

2. Comparison of time period

Comparing Case $PC^{=}T^{=}A^{2.85}$ with Case $PC^{=}T^{+}A^{3.15}$, which represented a 10% slower T1 and T2, the variation in the plasma fluid properties were smaller than those due to the 10% variation in peak current, (less than 1%) Table 3, and reduced each of the peak magnitudes (temperature, pressure and velocity). Peak plasma temperature and velocity occurred 0.1ms later for Case $PC^{=}T^{+}A^{3.15}$ however, interestingly, peak pressure occurred marginally earlier (0.02ms) for Case $PC^{=}T^{+}A^{3.15}$.

At the specimen surface the magnitude of the variations were similar to those found when peak current was changed (< 6.2%). However, surface temperature was slightly higher for the slower case ($PC^{=}T^{+}A^{3.15}$). Peak surface pressure occurred 0.21mm closer to the center of the arc despite Case $PC^{=}T^{+}A^{3.15}$ being a slower waveform while peak surface velocity and current density occurred at the same radius in both cases. This was due to the effect of marginally higher surface and near equal plasma velocities.

Comparing Case $PC^{+}T^{=}A^{3.44}$ with Case $PC^{+}T^{+}A^{3.82}$, which was 10% slower, but both with increased peak currents, again the overall variation within the plasma was lower than due to peak current change. The maximum change in plasma properties was only 6.9% (pressure). In this pairing the peak plasma properties all occurred on average 0.05ms later for Case $PC^{+}T^{+}A^{3.82}$. The variation at specimen surface level ranged from -3.76% to 6.43%. Surface pressure was the only load with a different radial position, 0.98mm closer to the arc center for Case $PC^{+}T^{+}A^{3.82}$.

3. Comparison of combined time period and peak current effects

Case $PC^{+}T^{+}A^{3.82}$ had higher plasma properties than Case $PC^{=}T^{=}A^{2.85}$. However comparing Case $PC^{+}T^{+}A^{3.82}$ with $PC^{+}T^{=}A^{3.44}$ plasma peak temperature and pressure were similar and peak surface pressure was lower. Comparing an increase in peak current with an increase in both peak current and time periods

an interesting pattern and outlier emerged as seen in Table 4. The percentage increase resulting from one or both factors was comparable except for plasma pressure which increased by 12% with peak current but only 4.2% with both peak current and time period. At the surface a similar trend was observed. As surface temperature and velocity increased significantly with the modification of both factors compared to peak current only, surface pressure actually reduced (compared with the base case, $PC^{=}T^{=}A^{2.85}$). This result appeared to be an outlier however investigation of the correlation between waveform properties, plasma properties and specimen loads would provide some explanation.

4. Correlating plasma properties and specimen loading with waveform parameters

Table 6 presents the correlation data for the Waveform parameters vs plasma properties and specimen loading. Each property and load measure is discussed in turn, in the context of the effect of each waveform parameter.

Peak current had a very strong positive relationship with the peak fluid temperature, pressure and velocity with values of 1.0, 0.84 and 1.0 and surface velocity and surface current density, with values of 0.89 and 1.0, respectively. However, for surface pressure (0.34) and temperature (0.5) there was only a moderate positive linear relationship. There was strong correlation between the surface loads and both action integral and charge transfer. However, there was weak negative linear correlation calculated between action integral, charge transfer and the specimen surface pressure.

Strong negative linear correlation was calculated between time periods (T1/T2) and specimen peak surface pressure (-0.92) while there was only a moderate negative linear correlation calculated between T1/T2 and the plasma pressure (-0.42). In fact T1/T2 had some negative correlation with all plasma properties bar surface velocity and temperature.

Clearly there was a disproportionate variation between the plasma properties due to the 10% variation in waveform properties. However, peak current, action integral and charge transfer were strongly linked but the outliers again are related to pressure. Peak current had a strong, positive linear relationship with fluid pressure (0.84) while action integral and charge transfer had only moderate linear correlations (0.52 and 0.37). Even more interesting was at the surface where the correlations reduced to 0.34, -0.15 and -0.32. From these results there was clearly a highly non-linear relationship between waveform properties and the associated plasma and surface peak pressures which requires further study.

5. Comparison of plasma observations with experiments

The work of Sonehara et al. [40], for scaled Waveform A, was used to benchmark the general trends found in these plasma simulations. Specimen A-1 (19.76kA) and A-2 (40.82kA) were used to discuss the effects of peak current since these represented a 107% increase in the waveform peak current parameter

with only a small variation in their waveform time periods (< 0.5%). The same conical electrode, probe-specimen surface offset of 2 mm and CFRP samples were used as the setup modelled herein.

The Schlieren photography results from Sonehara et al. were thus analyzed using image processing and converted to a simple arc profile of the edge of the hot gas region. Fig. 5 shows the resulting arcs for both tests at their individual waveform T1, T2 time points and at the end of the waveform. A similar approach was applied to the temperature contours for simulation cases $PC^{-}T^{-}A^{2.85}$ and $PC^{+}T^{-}A^{3.44}$ and an equivalent hot gas boundary identified and tracked, Fig. 5.

The scales in Fig. 5, from '0' to '100', represent the location from the arc center (located at '0') to the edge of the photograph or simulation domain (located at '100'). This analysis indicated that as the peak current increased, the hot gases and acoustic shock waves expanded more rapidly and the predicted plasma temperature increased for both the experiments and plasma simulations. Comparing the progress of the temperature profile along the x-axis there was generally similar behavior however, the extracted experimental data showed that the progress between T2 and End was approximately half as much as between T1 and T2. The simulations predicted a noteworthy difference in expansions between T2 and the end point which reduced by an approximate factor of 2.6. This was potentially due to the percentage change in waveform peak with the experiments increasing by 107% while simulations increased by 110% and also the inherent differences in total charge transfer and duration between Waveforms A and B.

6. Summary of simulated plasma behavior

In summary, peak current and action integral appear to be the factors which have the greatest influence on both the plasma properties and surface loads. With a fixed current duration, increasing the peak current of a waveform increased the applied action integral. An increase in peak current and action integral resulted in greater plasma peak temperature, pressure and velocity which were accompanied by an increase in specimen peak surface temperature, pressure and current density. However, the relationship between the plasma properties and the specimen surface loads was not a direct or simple one. That is to

say, a set percentage increase in plasma properties did not consistently lead to an increase in the peak magnitude witnessed at the specimen surface.

The thermal-electric damage predictions for the four case studies will now be discussed.

4.2 Damage results from thermal-electric simulations

Example output for the thermal-electric simulations is illustrated in Fig. 6 using case $PC^{+}T^{=}A^{3.44}$. The figure presents the temperature contour of the top ply, the severe damage outline for each of the top twelve plies and the through-thickness contours. Table 5 presents, for each thermal-electric simulation, the predicted damage depth, the predicted damage area (moderate and severe [22]) on the top ply (surface area) and the total specimen damage volume.

In general, when examining Table 5, greater peak current and action integral resulted in greater thermal damage depth. The increase in damage depth was accompanied by greater surface damage areas (moderate and severe) which together with greater depth resulted in an increase in total damage volume (again for moderate and severe damage). Increasing current duration (T1 and T2) again increased the damage depth, surface area and total volume (both moderate and severe) (comparing $PC^{=}T^{=}A^{2.85}$ and $PC^{=}T^{+}A^{3.15}$). Increasing both the peak current and the current duration simultaneously increased all the damage parameters. However, in this case the damage magnitudes were not consistently greater than those predicted when a single waveform parameter was varied (i.e. damage depth and severe damage area). Understanding this behavior required examination of the correlation coefficients.

4.3 Correlating damage with waveform parameters

Table 6 presents the correlation data for the Waveform parameters vs damage areas, volumes and depths. Each damage measure is discussed in turn, in the context of the effect of each waveform parameter.

Peak current variation was identified as having the greatest influence on the predicted severe damage area on the specimen surface (ply 1) and the predicted damage depth. Strong positive, linear correlations of 0.96 and 0.90, respectively, indicated that for a positive increase in peak current a near linear increase in the damage measure was expected as supported by the experimental work of Hirano et al. [1]. Peak current variation also impacted the predicted moderate (0.81) and severe (0.77) damage volumes and the moderate damage area (0.77) on the specimen surface (ply 1),

Table 6. The respective correlation coefficients indicated that for a positive increase in peak current an increase in each of these damage measures was expected, but the magnitude of increase did not follow a simple linear trend.

Waveform duration variation via T1/T2 had a smaller influence on the predicted damage than peak current variation. The greatest contribution of Waveform duration was on moderate damage area (ply 1) and both moderate and severe damage volumes with correlation coefficients of 0.61, 0.58 and 0.64, respectively. However, there were only moderate linear relationships between T1/T2 and the damage variables. The only negative correlation (-0.05) for T1/T2 was with severe damage area.

In general action integral and charge transfer had the strongest correlations with all damage measures bar one with correlations between 1.00 and 0.88 falling to 0.81/0.71 for ply 1 severe damage area. Simulation authors Dong et al. [42] and Yin et al. [43] and experimental author Kawakami [6] found that action integral was the best predictor of damage depth. Action integral had the greatest correlation with moderate damage area (0.98), a result also observed experimentally by Hirano et al. [1] and numerically by Dong et al. [42] and Yin et al. [43]. These observed correlations suggested a strong positive linear relationship between action integral and charge transfer and the studied damage measures.

Finally, correlations existed between the damage measures due to the relationship between damage area at the specimen surface, damage depth and damage volume. There was very strong, positive linear correlation (0.94) between severe damage area and damage depth. This presented a potential method to predict damage depth from the surface severe damage area. However, experiments would be required to confirm this behavior and whether it could be expanded beyond Waveform B.

1. Linearity assessment

In addition to correlation factors the output data points from Table 3, Table 4, and Table 5 were plotted and the R^2 determined using a linear line of best fit. Table 7 shows the R^2 values for each plasma property,

surface load and damage metric against each waveform parameter. This data helped to determine if the trends were likely to be linear or non-linear.

Generally speaking the relationships between waveform rise and fall (T1/T2) and the plasma property, surface load and damage metric appeared to be non-linear. Only the outputs of specimen surface pressure and temperature had R^2 values equal to or above 0.75 respectively. Action integral had a potentially linear relationship with moderate damage area and moderate and severe damage volumes (0.96, 0.98 and 0.96 respectively) - a result supported by Kawakami [6]. Peak current also had a potentially linear relationship with peak plasma temperature and velocity with R^2 values of 0.99 in both cases. Action integral and charge had broadly similar R^2 values for each metric however action integral was generally slightly higher.

As with the absolute values discussed previously, plasma and surface pressure stood out. Both of these metrics appeared to be non-linear with both action integral and charge while surface pressure varied non-linearly with peak current. However, plasma fluid pressure appeared to vary linearly with peak current. This finding provided more evidence that the interaction of waveform properties and plasma/surface pressure requires further investigation; however, a faster and more computationally efficient simulation should be used for this.

5.0 Conclusions

This paper attempted to quantify the influence of varying the waveform parameters on the predicted plasma behavior and resulting specimen damage produced during an artificial lightning strike using test Waveform B. The plasma behavior was represented using a Magnetohydrodynamic FE multiphysics model and the specimen behavior was represented using a FE thermal-electric model.

The analysis results demonstrated that:

- Peak current (and action integral, transfer charge) were the key factors influencing both the plasma properties (12% increase in plasma peak pressure) and the specimen damage (15.2% increase in thermal damage depth).

- Based on the limited number of plasma simulations the effects of peak current and action integral on the plasma properties and damage appeared to be linear (minimum R^2 value of 0.96).
- In general waveform peak current was the most influential parameter examined.
- For peak specimen surface load magnitudes, the most influential parameter found for pressure and temperature was waveform T1/T2 (correlations of -0.92 and 0.86 respectively).
- For specimen current density the most influential parameter found was waveform peak current (correlation of 1.00).
- Considering specimen damage, the majority of the damage measurements had the strongest correlations with waveform peak current.
- The effect of time period variation on damage appeared to be potentially non-linear (max R^2 of 0.37), requiring additional study.

Since only four simulation data sets have been used herein, additional simulation data, for example considering each factor at three levels, could be used to refine the understanding of the relationships. However, to do this less expensive plasma simulations are required as the plasma simulations herein took approximately ten days each to complete. The results of this work can be used to achieve greater understanding of the interaction of artificial lightning with aircraft structures and can be used to guide aircraft design through the development of advanced lightning strike protection systems.

Acknowledgements

Financial support from The Engineering and Physical Sciences Research Council (EPSRC) for the Ph.D. research of S.L.J. Millen is gratefully acknowledged.

References

[1] Y. Hirano, S. Katsumata, Y. Iwahori, and A. Todoroki, "Artificial lightning testing on graphite/epoxy composite laminate," *Compos. Part A Appl. Sci. Manuf.*, vol. 41, no. 10, pp. 1461–1470, 2010.

[2] S. Eliezer and Y. Eliezer, *The Fourth State of Matter - An Introduction to Plasma Science*, 2nd ed. Bristol: Institute of Physics Publishing, 2001.

[3] SAE Aerospace, "Aerospace Recommended Practice ARP5412B," 1999.

[4] P. Feraboli and H. Kawakami, "Damage of Carbon/Epoxy Composite Plates Subjected to Mechanical Impact and Simulated Lightning," *J. Aircr.*, vol. 47, no. 3, pp. 999–1012, 2010.

[5] J. Sun, X. Yao, X. Tian, J. Chen, and Y. Wu, "Damage Characteristics of CFRP Laminates Subjected to Multiple Lightning Current Strike," *Appl. Compos. Mater.*, 2018.

[6] H. Kawakami, "Lightning Strike Induced Damage Mechanisms of Carbon Fiber Composites," Washington, 2011.

[7] F. Moupfouma, "Aircraft Structure Paint Thickness and Lightning Swept Stroke Damages," *SAE Int. J. Aerosp.*, vol. 6, no. 2, pp. 392–398, 2013.

[8] J. Morgan, "Thermal Simulation and Testing of Expanded Metal Foils Used for Lightning Protection of Composite Aircraft Structures," *SAE Int. J. Aerosp.*, vol. 6, no. 2, pp. 371–377, 2013.

[9] F. Moupfouma, Z. Klim, and A. Skorek, "Electromagnetic Protection Hazards on Composite versus Metallic Aircraft," *SAE Int. J. Aerosp.*, vol. 6, no. 2, pp. 441–446, 2013.

[10] M. J. Kofoid, "Lightning discharge heating of aircraft skins," *J. Aircr.*, vol. 7, no. 1, pp. 21–26, 2008.

[11] Y. Kostogorova-Beller, "Physics of Interaction of Lightning Currents with Aluminum Sheets," *J. Aircr.*, vol. 49, no. 1, pp. 66–75, 2012.

[12] Y. Kostogorova-Beller and F. S. Diatchkovski, "Quantification of the Material's Resistance to Damage by Lightning," *J. Aircr.*, vol. 50, no. 3, pp. 827–831, 2013.

[13] N. Hosokawa, T. Ooto, S. Kubo, M. Anzai, A. Yoshiya, and A. Nakagoshi, "Lightning Strike Protection for Composite Laminates by Pitch-Based Carbon Fibre Skin," in *International Conference on Composite Materials*, 2013, pp. 1–10.

[14] S. J. Haigh, "Impulse Effects during Simulated Lightning Attachments to Lightweight Composite Panels," in *Int. Aerospace and Ground Conf. on Lightning and Static Electricity*, 2007, pp. 1–21.

[15] Q. Dong *et al.*, "Damage analysis of carbon fiber composites exposed to combined lightning current components D and C," *Compos. Sci. Technol.*, vol. 179, pp. 1–9, 2019.

[16] P. Feraboli and M. Miller, "Damage resistance and tolerance of carbon/epoxy composite coupons subjected to simulated lightning strike," *Compos. Part A Appl. Sci. Manuf.*, vol. 40, no. 6–7, pp. 954–967, 2009.

[17] R. Muñoz, S. Delgado, C. González, B. López-Romano, D. Y. Wang, and J. Llorca, "Modeling lightning impact thermo-mechanical damage on composite materials," *Appl. Compos. Mater.*, vol. 21, no. 1, pp. 149–164, 2014.

[18] S. L. J. Millen, A. Murphy, G. Catalanotti, and G. Abdelal, "Coupled thermal-mechanical progressive damage model with strain and heating rate effects for lightning strike damage assessment," *Appl. Compos. Mater.*, vol. 26, no. 5, pp. 1437–1459, 2019.

[19] F. Wang, X. Ma, H. Chen, and Y. Zhang, "Evolution simulation of lightning discharge based on a magnetohydrodynamics method," *Plasma Sci. Technol.*, vol. 20, no. 7, 2018.

[20] T. Ogasawara, Y. Hirano, and A. Yoshimura, "Coupled thermal-electrical analysis for carbon fiber/epoxy composites exposed to simulated lightning current," *Compos. Part A Appl. Sci. Manuf.*, vol. 41, no. 8, pp. 973–981, 2010.

[21] S. L. J. Millen, A. Murphy, G. Abdelal, and G. Catalanotti, "Specimen Representation on the Prediction of Artificial Test Lightning Plasma, Resulting Specimen Loading and Subsequent Composite Material Damage," *Compos. Struct.*, vol. 231C, 2019.

[22] P. Foster, G. Abdelal, and A. Murphy, "Understanding how arc attachment behaviour influences the prediction of composite specimen thermal loading during an artificial lightning strike test,"

Compos. Struct., vol. 192, pp. 671–683, 2018.

[23] Q. Dong, G. Wan, L. Ping, Y. Guo, X. Yi, and Y. Jia, "Coupled thermal-mechanical damage model of laminated carbon fiber/resin composite subjected to lightning strike," *Compos. Struct.*, vol. 206, pp. 185–193, 2018.

[24] H. Chen, F. S. Wang, X. T. Ma, and Z. F. Yue, "The coupling mechanism and damage prediction of carbon fiber/epoxy composites exposed to lightning current," *Compos. Struct.*, vol. 203, pp. 436–445, 2018.

[25] G. F. Abdelal and A. Murphy, "Nonlinear numerical modelling of lightning strike effect on composite panels with temperature dependent material properties," *Compos. Struct.*, vol. 109, no. 1, pp. 268–278, 2014.

[26] G. F. Abdelal and A. Murphy, "A multiphysics simulation approach for efficient modeling of lightning strike tests on aircraft structures," *IEEE Trans. Plasma Sci.*, vol. 45, no. 4, pp. 725–735, 2017.

[27] H. G. Fan, Y. W. Shi, and S. J. Na, "Numerical analysis of the arc in pulsed current gas tungsten arc welding using a boundary-fitted coordinate," *J. Mater. Process. Technol.*, vol. 72, pp. 437–445, 1997.

[28] F. Lago, J. J. Gonzalez, P. Freton, and A. Gleizes, "A numerical modelling of an electric arc and its interaction with the anode: Part I. The two-dimensional model," *J. Phys. D. Appl. Phys.*, vol. 37, no. 6, pp. 883–897, 2004.

[29] F. Lago, J. J. Gonzalez, P. Freton, F. Uhlig, N. Lucius, and G. P. Piau, "A numerical modelling of an electric arc and its interaction with the anode: part III. Application to the interaction of a lightning strike and an aircraft in flight," *J. Phys. D. Appl. Phys.*, vol. 39, no. 10, pp. 2294–2310, 2006.

[30] M. Tanaka, H. Terasaki, M. Ushio, and J. J. Lowke, "A Unified Numerical Modeling of Stationary Tungsten-Inert- Gas Welding Process," *Metall. Mater. Trans. A*, vol. 33, no. July, pp. 2043–2052, 2002.

[31] M. Tanaka and J. J. Lowke, “Predictions of weld pool profiles using plasma physics,” *J. Phys. D. Appl. Phys.*, vol. 40, pp. R1–R23, 2006.

[32] L. Sansonnens, J. Haidar, and J. J. Lowke, “Prediction of properties of free burning arcs including effects of ambipolar diffusion,” *J. Phys. D. Appl. Phys.*, vol. 33, no. 2, pp. 148–157, 1999.

[33] J. J. Lowke, R. Morrow, and J. Haidar, “A simplified unified theory of arcs and their electrodes,” *J. Phys. D. Appl. Phys.*, vol. 30, no. 14, pp. 2033–2042, 1997.

[34] A. Traidia and F. Roger, “Numerical and experimental study of arc and weld pool behaviour for pulsed current GTA welding,” *Int. J. Heat Mass Transf.*, vol. 54, no. 9–10, pp. 2163–2179, 2011.

[35] S. L. J. Millen, A. Murphy, G. Abdelal, and G. Catalanotti, “Sequential finite element modelling of lightning arc plasma and composite specimen thermal-electric damage,” *Comput. Struct.*, vol. 222, pp. 48–62, 2019.

[36] P. Foster, G. Abdelal, and A. Murphy, “Quantifying the Influence of Lightning Strike Pressure Loading on Composite Specimen Damage,” *Appl. Compos. Mater.*, vol. 26, no. 1, pp. 115–137, 2018.

[37] P. Foster, G. Abdelal, and A. Murphy, “Modelling of mechanical failure due to constrained thermal expansion at the lightning arc attachment point in carbon fibre epoxy composite material,” *Eng. Fail. Anal.*, vol. 94, pp. 364–378, 2018.

[38] A. G. Asuero, A. Sayago, and A. G. González, “The correlation coefficient: An overview,” *Crit. Rev. Anal. Chem.*, vol. 36, no. 1, pp. 41–59, 2006.

[39] B. Ratner, “The correlation coefficient: Its values range between +1/-1, or do they?,” *J. Targeting, Meas. Anal. Mark.*, vol. 17, no. 2, pp. 139–142, 2009.

[40] T. Sonehara, H. Kusano, N. Tokuoka, and Y. Hirano, “Visualization of lightning impulse current discharge on CFRP laminate,” in *2014 International Conference on Lightning Protection, ICLP 2014*, 2014, vol. 4, pp. 835–839.

[41] Q. Dong, Y. Guo, X. Sun, and Y. Jia, “Coupled electrical-thermal-pyrolytic analysis of carbon fiber/epoxy composites subjected to lightning strike,” *Polym. (United Kingdom)*, vol. 56, pp. 385–

394, 2015.

[42] Q. Dong *et al.*, “Influencing factor analysis based on electrical-thermal-pyrolytic simulation of carbon fiber composites lightning damage,” *Compos. Struct.*, vol. 140, pp. 1–10, 2016.

[43] J. J. Yin, F. Chang, S. L. Li, X. L. Yao, J. R. Sun, and Y. Xiao, “Lightning Strike Ablation Damage Influence Factors Analysis of Carbon Fiber/Epoxy Composite Based on Coupled Electrical-Thermal Simulation,” *Appl. Compos. Mater.*, no. 1, pp. 1–18, 2016.

[44] ABAQUS 2016 Documentation, *Abaqus User Subroutines Reference Guide*. 2017.

Table 1 Idealized lightning current component waveform norm values derived from Ref. [3] and using Design of Experiments for Plasma Simulations.

Test Case	Peak Current (kA)	Time to Peak / T1 (μs)	Time to Half-Value / T2 (μs)	Percentage Change in Peak Current/T1/ T2 (%)	Action Integral (A^2s)	Percentage Change in Action Integral (%)	Charge Transfer (C)	Percentage Change in Charge Transfer (%)
$PC^{=}T^{=}A^{2.85}$	4.17	813	2345	-	$2.85x10^4$	-	10.0	-
$PC^{+}T^{=}A^{3.44}$	4.59	813	2345	0	$3.44x10^4$	+20.0	11.0	+10.0
$PC^{=}T^{+}A^{3.15}$	4.17	894	2605	+10	$3.15x10^4$	+10.5	10.8	+8.0
$PC^{+}T^{+}A^{3.82}$	4.59	894	2605	+10	$3.82x10^4$	+34.0	11.9	+19.0

*Percentage change measured against original simulation

Table 2 Temperature dependent CFRP material properties

Temperature dependent material properties				
		Thermal Conductivity		
Temperature (°C)	Specific Heat (J/kg°C)	Fibre (W/mm.K)	Transverse (W/mm.K)	Through-Thickness (W/mm.K)
25	1065	0.008	0.00067	0.00067
500	2100	0.004390	0.000342	0.000342
800	2100	0.002608	0.00018	0.00018
1000	2171	0.001736	0.0001	0.0001
3316	2500	0.001736	0.0001	0.0001
3334*	5875	0.001736	0.0001	0.0001
3335*	5875	0.0005	0.0005	0.0005
7000*	5875	0.001015	0.001015	0.001015
		Electrical Conductivity		
Temperature (°C)	Density (kg/mm^3)	Fibre (1/ Ω.mm)	Transverse (1/ Ω.mm)	Through-Thickness (1/ Ω.mm)
25	$1.52x10^{-6}$	35.97	0.001145	$1.79x10^{-6}$
500	$1.52x10^{-6}$	35.97	0.001145	$1.79x10^{-6}$
800	$1.10x10^{-6}$	35.97	0.001145	$1.79x10^{-6}$
3316	$1.10x10^{-6}$	35.97	0.001145	$1.79x10^{-6}$
3334*	$1.11x10^{-9}$	35.97	2	$1x10^{6}$
3335*	$1.11x10^{-9}$	0.2	0.2	$1x10^{6}$
7000*	$1.11x10^{-9}$	1.5	1.5	$1x10^{6}$
* - Gas				

	Temperature Range (°C)	Energy Released (J)
Resin Decomposition	500-800	$4.8x10^{6}$
Fiber Ablation	3316-3334	$43x10^{6}$

Table 3 Output summary for plasma

Test Case	Peak Current (kA)	T1 (µs)	T2 (µs)	Action Integral ($x10^4$ A^2s)	Charge Transfer (C)	Peak Fluid Properties and Percentage Change					
						Temperature (K / ±%)		Pressure (Pa / ±%)		Velocity (m/s / ±%)	
$PC^{-}T^{-}A^{2.85}$	4.17	813	2345	2.85	10.0	34,051	-	187,160	-	2077	-
$PC^{+}T^{-}A^{3.44}$	4.59	813	2345	3.44	11.0	34,391	+1.00	209,660	+12.0	2180	+4.96
$PC^{-}T^{+}A^{3.15}$	4.17	894	2605	3.15	10.8	34,042	-0.03	185,770	-0.74	2069	-0.39
$PC^{+}T^{+}A^{3.82}$	4.59	894	2605	3.82	11.9	34,394	+1.01	195,090	+4.24	2172	+4.57

Table 4 Output summary for specimen surface loads

Test Case	Peak Current (kA)	T1 (μs)	T2 (μs)	Action Integral (x10^4 A^2s)	Charge Transfer (C)	Peak Specimen Surface Loads and Percentage Change						
						Temperature (K / ±%)		Pressure (Pa / ±%)		Velocity (m/s / ±%)		Current Density (A/mm^2 / ±%)
$PC^{=}T^{=}A^{2.85}$	4.17	813	2345	2.85	10.0	4620.1	-	123,070	-	25.0	-	44.3
$PC^{+}T^{=}A^{3.44}$	4.59	813	2345	3.44	11.0	4782.0	+3.5	125,280	+1.8	27.3	+9.2	46.5
$PC^{=}T^{+}A^{3.15}$	4.17	894	2605	3.15	10.8	4906.8	+6.2	119,890	-2.6	26.1	+4.4	44.3
$PC^{+}T^{+}A^{3.82}$	4.59	894	2605	3.82	11.9	5089.7	+10.2	120,570	-2.0	28.6	+14	46.5

Table 5 Output summary for thermal damage

Test Case	Peak Current (kA)	T1 (μs)	T2 (μs)	Action Integral (x10^4 A^2s)	Charge Transfer (C)	Specimen Damage Summary and Percentage Change									
						Damage Depth			Moderate Damage Area		Severe Damage Area		Moderate Damage Volume		Severe Damage Volume	
						Plies	mm	(±%)	(mm^2)	(±%)	(mm^2)	(±%)	(mm^3)	(±%)	(mm^3)	(±%)
$PC^{=}T^{=}A^{2.85}$	4.17	813	2345	2.85	10.0	13	1.91	-	3661	-	1372	-	2082	-	726	-
$PC^{+}T^{=}A^{3.44}$	4.59	813	2345	3.44	11.0	15	2.20	+15.2	3680	+0.52	1398	+1.90	2228	+7.01	789	+8.68
$PC^{=}T^{+}A^{3.15}$	4.17	894	2605	3.15	10.8	14	2.06	+7.90	3675	+0.38	1377	+0.36	2180	+4.71	777	+7.02
$PC^{+}T^{+}A^{3.82}$	4.59	894	2605	3.82	11.9	15	2.20	+15.2	3706	+1.23	1391	+1.38	2371	+13.9	856	+17.9

Table 6 Correlation matrix for Waveform Parameters, Plasma Fluid Properties, Specimen Surface Loads and Predicted Damage

		Waveform inputs			*Waveform outputs*		*Plasma Fluid*			*Specimen Surface Outputs*				*Specimen Damage Outputs*				
		Peak Current	*T1*	*T2*	*A.I.*	*Charge*	*Temp.*	*Pressure*	*Velocity*	*Pressure*	*Velocity*	*Temp.*	*Current*	*Mod. Area*	*Sev. Area*	*Mod. Vol*	*Sev. Vol*	*Depth*
Waveform inputs	*Peak Current*	1.00														Correlation coefficient (C.C.) color key:		
	T1	0.00	1.00													C.C. = 1.00		
	T2	0.00	1.00	1.00												1.00 >C.C.≥ 0.95		
Waveform outputs	*A.I.*	0.88	0.47	0.47	1.00											0.95 >C.C.≥ 0.90		
	Charge	0.78	0.63	0.63	0.98	1.00										0.90 >C.C.≥ 0.85		
Plasma fluid	*Temp.*	1.00	-0.01	-0.01	0.88	0.77	1.00									0.85 >C.C.> 0.00		
	Pressure	0.84	-0.42	-0.42	0.52	0.37	0.84	1.00								C.C. = 0.00		
	Velocity	1.00	-0.08	-0.08	0.84	0.73	1.00	0.87	1.00							-0.85 < C.C.< 0.00		
Specimen surface outputs	*Pressure*	0.34	-0.92	-0.92	-0.15	-0.32	0.34	0.73	0.41	1.00						-0.90 <C.C.< -0.85		
	Velocity	0.89	0.45	0.45	1.00	0.98	0.89	0.55	0.86	-0.12	1.00					-0.95 <C.C.< -0.90		
	Temp.	0.50	0.86	0.86	0.85	0.93	0.49	0.05	0.43	-0.63	0.84	1.00				-1.00 ≤C.C.< -0.95		
	Current	1.00	0.00	0.00	0.88	0.78	1.00	0.84	1.00	0.34	0.89	0.50	1.00			C.C. = -1.00		
Specimen damage outputs	*Mod. Area*	0.77	0.61	0.61	0.98	0.99	0.77	0.33	0.72	-0.33	0.97	0.92	0.77	1.00				
	Sev. Area	0.96	-0.05	-0.05	0.81	0.71	0.96	0.92	0.96	0.42	0.83	0.43	0.96	0.66	1.00			
	Mod. Vol	0.81	0.58	0.58	0.99	1.00	0.81	0.40	0.76	-0.28	0.99	0.91	0.81	1.00	0.72	1.00		
	Sev. Vol	0.77	0.64	0.64	0.98	1.00	0.76	0.35	0.71	-0.34	0.97	0.94	0.77	0.99	0.68	1.00	1.00	
	Depth	0.90	0.30	0.30	0.92	0.88	0.90	0.74	0.88	0.08	0.93	0.71	0.90	0.83	0.94	0.87	0.86	1.00

Table 7 R^2 values for linear plots of waveform properties vs. plasma properties/predicted damage metrics (no units)

	Peak Plasma Temp.	Peak Plasma Pressure	Peak Plasma Velocity	Peak Surface Temp.	Peak Surface Pressure	Peak Surface Velocity	Peak Surface Current	Ply 1 Moderate Area	Ply 1 Severe Area	Moderate Damage Vol.	Severe Damage Vol.	Damage Depth
Peak Current	0.99	0.70	0.99	0.25	0.11	0.80	1.00	0.60	0.93	0.65	0.59	0.82
T1/T2	0.00	0.18	0.01	0.75	0.85	0.20	0.00	0.37	0.00	0.33	0.41	0.09
Action Integral	0.77	0.27	0.70	0.73	0.02	0.99	0.77	0.96	0.65	0.98	0.96	0.85
Charge Transfer	0.59	0.14	0.53	0.87	0.11	0.95	0.60	0.98	0.50	0.99	0.99	0.78

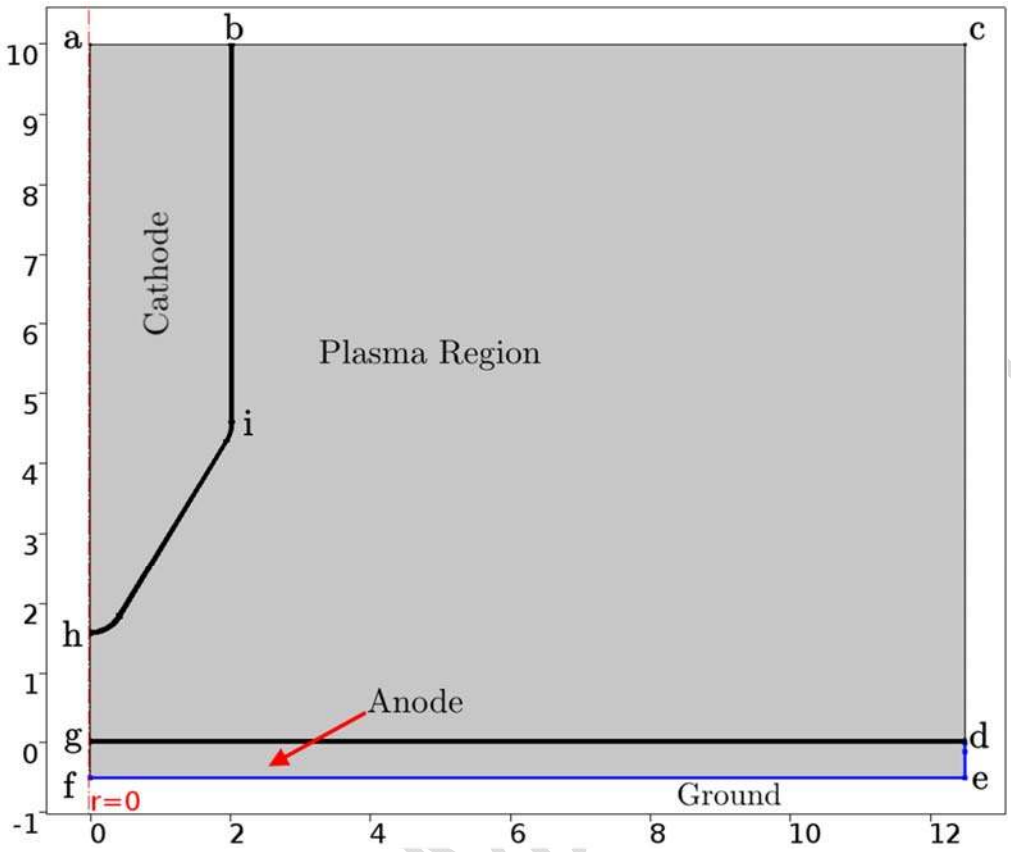

Fig. 1 Plasma simulation domain

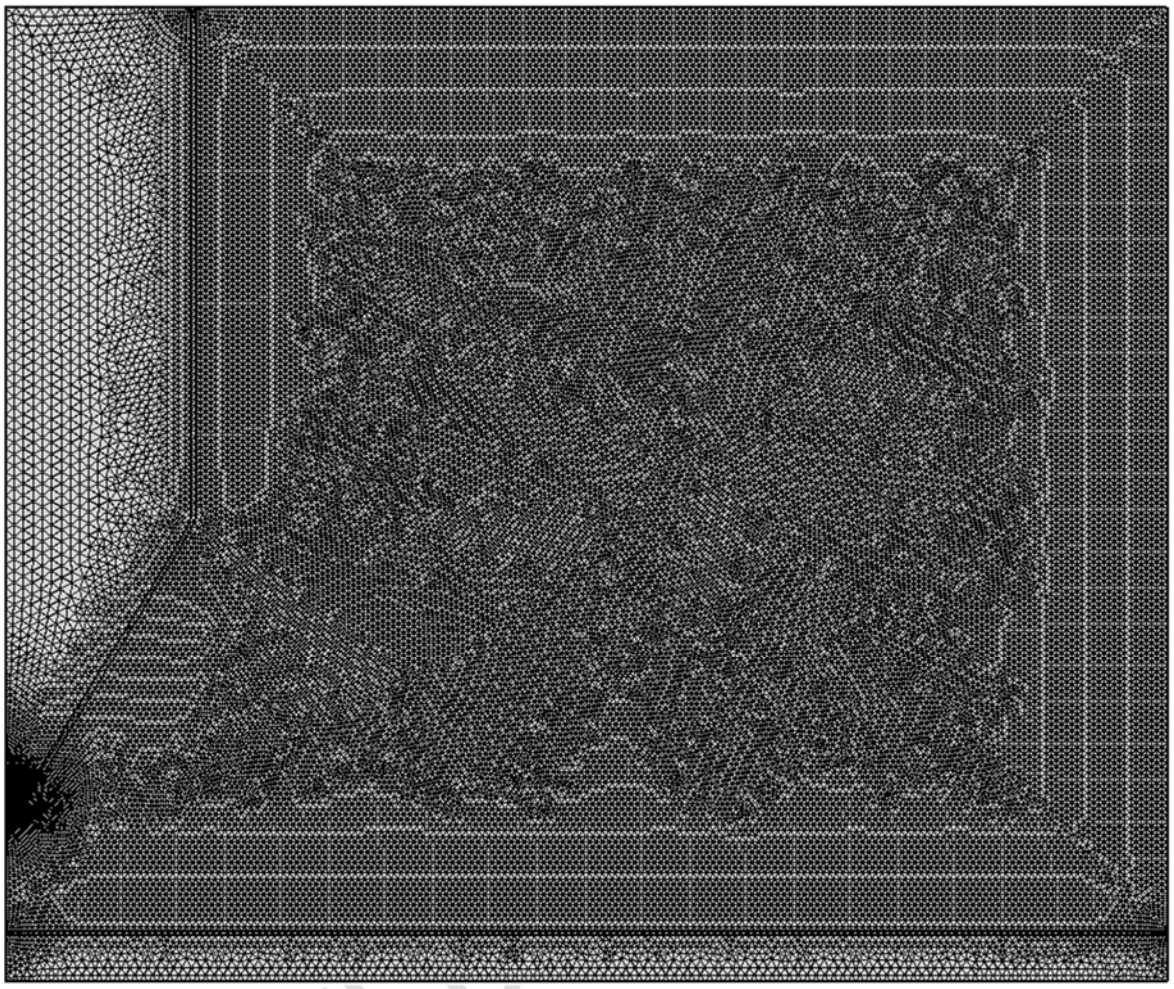

Fig. 2 Plasma simulation mesh

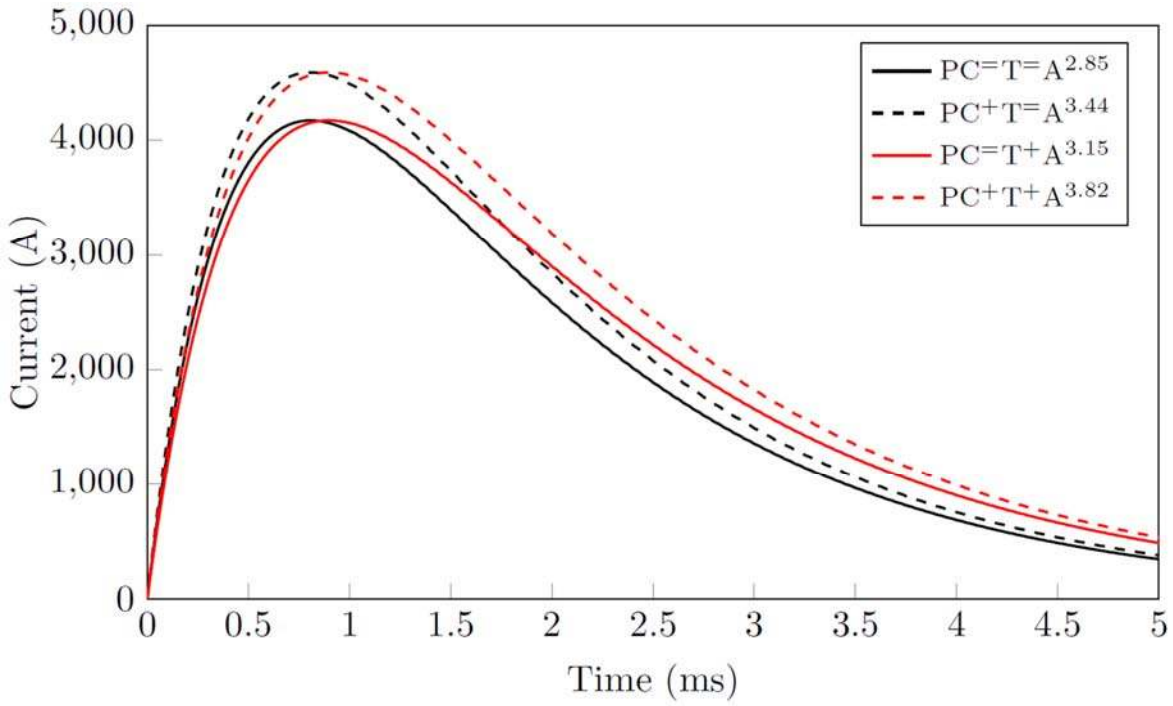

Fig. 3 Plasma simulation input waveforms

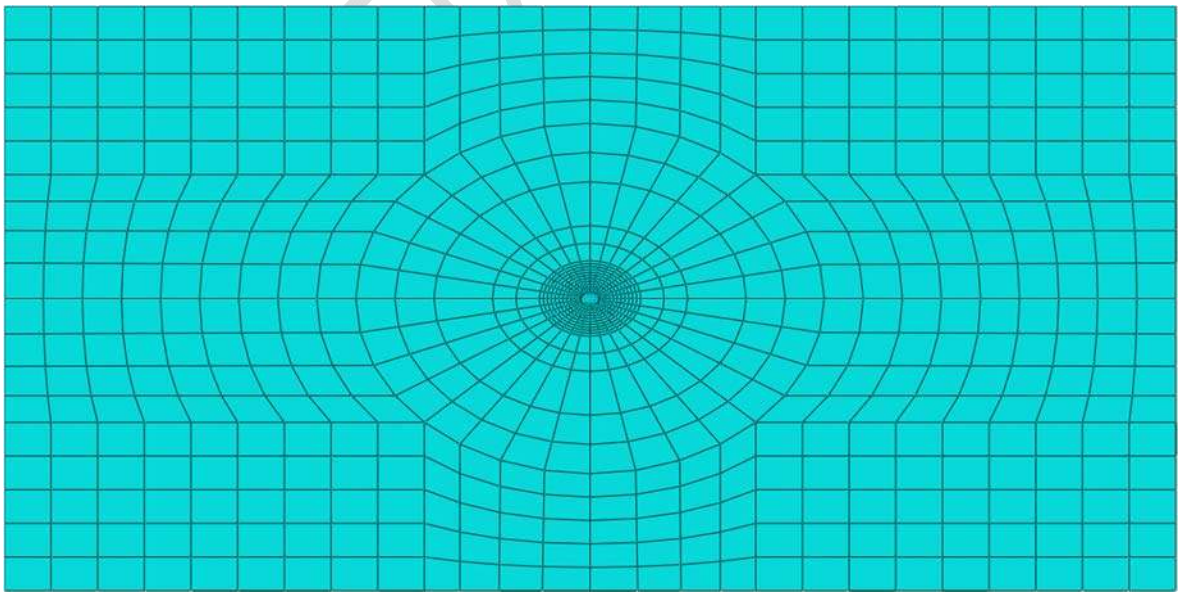

Fig. 4 Final mesh used in thermal-electric simulations

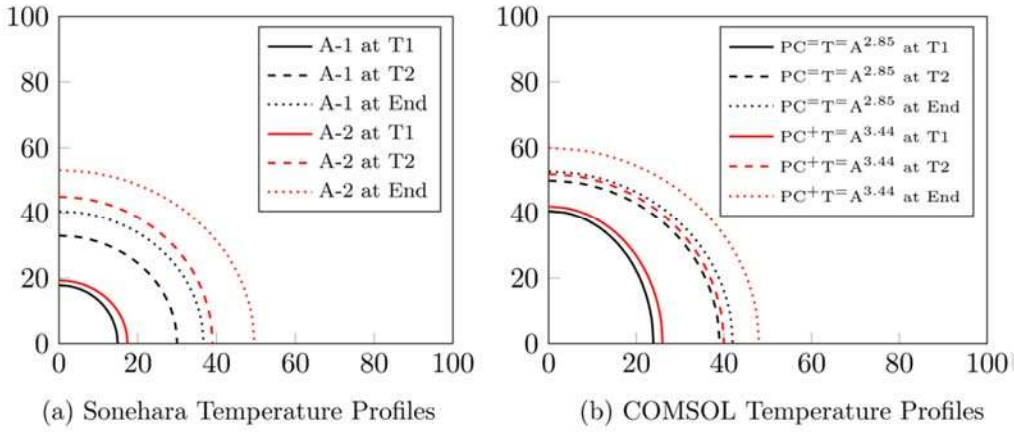

Fig. 5 Plasma temperature contour outlines from Sonehara et al.[40] **and this work where A-1 is 19.76kA, A-2 is 40.82kA, $PC^{=}T^{=}A^{2.85}$ is 4.17kA and $PC^{+}T^{=}A^{3.44}$ is 4.59kA**

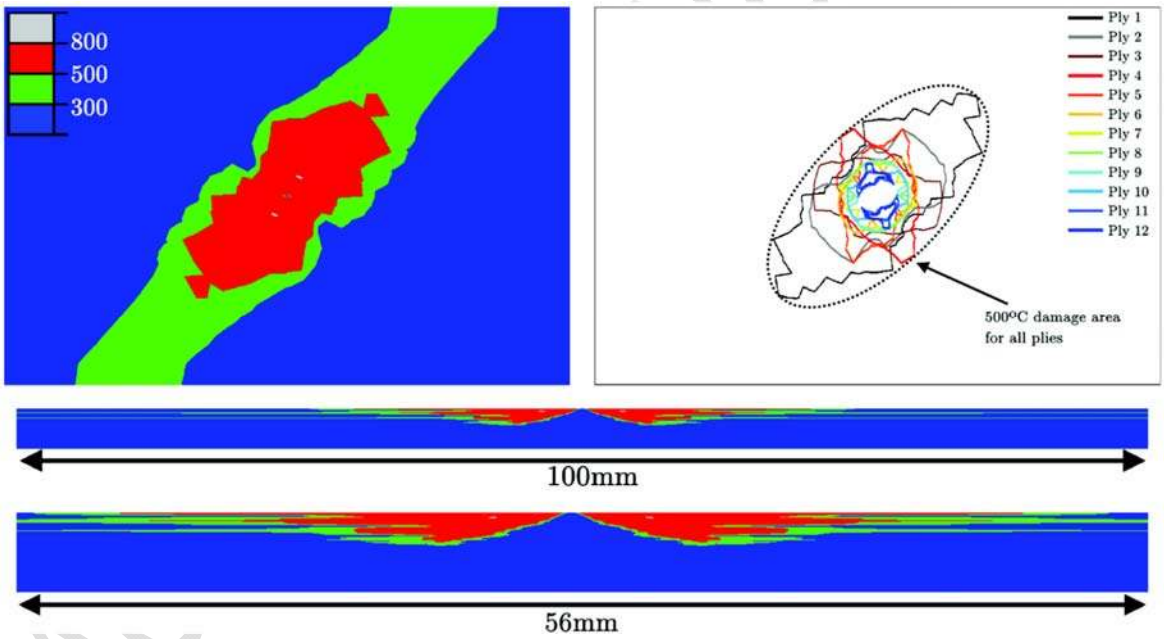

Fig. 6 Temperature contours and severe damage outlines for $PC^{+}T^{=}A^{3.44}$